Selective gas adsorption by calixarene-based porous octahedral M_{32} coordination cages

Ivan V. Khariushin, Alexander S. Ovsyannikov,* Stéphane Baudron, Jas S. Ward, Anniina Kiesilä, Kari Rissanen, Elina Kalenius, Konstantin A. Kovalenko, Vladimir P. Fedin, Svetlana E. Solovieva, Igor S. Antipin, Véronique Bulach and Sylvie Ferlay*

Synthesis

General: All reagents and solvents were of analytical grade and purchased from commercial sources and were used without further purification. The synthesis of (**1**-4H) was adapted from an already reported procedure.[1] The synthesis and characterization of racemic metalloconnector $(Co^{III}L_3)^{3+}$ (L = 5-(4-carboxyl- phenyl)-4,6-dipyrrinato)) was performed as previously described.[2,3]

Crystallisation of 2 (*$Co^{II}_{24}Co^{III}_8$*)

Tris[5-(4-Carboxyphenyl)-4,6-dipyrrinato]Co(III) (0.0296g, 0.031 mmol), sulfonylcalix[4]arene (0.020g, 0.023 mmol) and cobalt (II) chloride hexahydrate (0.0224g, 0.094 mmol) were dissolved in 5 ml of DMF and then were put in a tube. Mixture of 1 ml of MeOH and 1 ml of DMF were placed in the tube above DMF solution. Triethylamine (0.033 ml, 0.23 mmol) was dissolved in 3 ml of MeOH. Triethylamine solution was placed in the tube above mixture of DMF and MeOH. The tube was sealed and left for a week. Octahedral red crystals suitable for further analysis were collected via filtration. Yield = 0.045g (86 %). Anal. Found for $C_{624}H_{504}Co_{32}N_{48}O_{126}S_{24}$(13250.41) : C, 52.52; H, 5.05; N, 7.48 %. Calc. C, 56.88; H, 4.05 N, 5.01%. ESI-MS : $[M^{6-}]$ = 2227.6159. IR (KBr, cm^{-1})ϑ : 563(m), 623(w), 659(m), 724(m), 780(m), 794(m), 830(m), 891(m), 901(w), 1000(s), 1029(s), 1033(s), 1082(m), 1132(m), 1143(w), 1204(m), 1249(s), 1289(m), 1345(s), 1379(s), 1387(s), 1456(m), 1490(s), 1560(s), 1604(m), 1662(s), 1736(w), 2865(w), 2951(m), (see figure S3)

Crystallisation of 3 (*$Ni^{II}_{24}Co^{III}_8$*)

Tris[5-(4-Carboxyphenyl)-4,6-dipyrrinato]Co(III) (0.0296g, 0.031 mmol), sulfonylcalix[4]arene (0.020g, 0.023 mmol) and nickel (II) chloride hexahydrate (0.0224g, 0.094 mmol) were dissolved in 5 ml of DMF and then were put in a tube. Mixture of 1 ml of MeOH and 1 ml of DMF were placed in the tube above DMF solution. Triethylamine (0.033 ml, 0.23 mmol) was dissolved in 3 ml of MeOH. Triethylamine solution was placed in the tube above mixture of DMF and MeOH. The tube was sealed and left for a week. Octahedral red crystals suitable for further analysis were collected via filtration. Yield = 0.041g (78 %). Anal. Found for $C_{624}H_{504}Ni_{24}Co_8N_{48}O_{126}S_{24}$ (13244.66) : C, 50.85; H, 5.64; N, 8.75 Calc. C, 56.90; H, 4.05 N, 5.01%. ESI-MS : $[M^{6-}]$ = 2224.4469; IR (KBr, cm^{-1})ϑ: 502(w), 566(m), 624(w), 722(m), 741(w), 778(m), 798(m), 831(m), 868(w), 890(m), 895(w), 1000(s), 1029(s), 1037(s), 1080(m), 1131(m), 1152(w), 1204(m), 1246(s), 1289(m), 1345(s), 1380(s), 1408(s), 1451(m), 1490(s), 1554(s), 1605(s), 1667(s), 2863(w), 2956(m), (see figure S4)

1 C.-M. Liu, D.-Q. Zhang, X. Hao, D.-B. Zhu, Syntheses, Crystal Structures, and Magnetic Properties of Two p-tert-Butylsulfonylcalix[4]arene Supported Cluster Complexes with a Totally Disordered Ln4(OH) 4Cubane Core. *Cryst. Growth Des*. **2012**, *12*, 2948-2954.

2 C. Brückner, Y. Zhang, S. J. Rettigand, D. Dolphin, Synthesis, derivatization and structural characterization of octahedral tris(5-phenyl-4,6-dipyrrinato) complexes of cobalt(Ill) and iron(m) *Inorg. Chim. Acta*, **1997**, *263*, 279-286.

3 S. J. Garibay, J. R. Stork, Z. Wang, S. M. Cohen, S. G. Telfer, Enantiopure *vs*. racemic metalloligands: impact on metal–organic framework structure and synthesis *Chem. Commun*., **2007**, 4881-4883.

Characterization techniques

The IR spectra of the polycrystalline samples were recorded on a Bruker Tensor 27 spectrometer (Bruker Optic GmbH, Germany) in KBr pellets. IR spectra are presented in Figures S3 and S4.

Elemental analysis was performed on a Vario Macro CHN Analyzer (Elementar Analysen systeme GmbH, Langenselbold, Germany).

ESI-MS and ion mobility mass spectrometry

Ion mobility mass spectrometry experiments were performed with Agilent 6560 ESI-IM-QTOF mass spectrometer equipped with dual AJS ion source and Drift Gas Upgrade Kit (Agilent Technologies, USA). Samples of racemic coordination cages **2** and **3** (0.005 g) were suspended in 250 µL of DCM, then filtrated and solution was diluted by 1 or 5 µL/ml of ACN. All measurements were done using negative mode (-)ESI on extended *m/z* range in with N_2 and He as a drift gases. The samples were injected into the ESI source with a flow rate of 5 µL min^{-1}. Dry gas temperature of 225 °C, drying gas flow rate 2 L min^{-1}, nebulizer pressure 5 psi, sheath gas temperature 225 °C, sheath gas flow 5 L min^{-1} were used. Capillary voltage of 4000 V, nozzle voltage of 2000 V and fragmentor voltage of 400 V were set as source parameters. In IM-MS experiments with N_2 drift gas, (He values in paranthesis), the drift tube pressure was set to 3.95 Torr and high-pressure funnel to 3.80 Torr (3.70 Torr). In the single-field IM experiments the drift tube entrance and exit voltages were set as 1574V (875V) and 224V (133V), respectively. Trap filling time of 10 000 µs (5000 µs) and trap release time of 150 µs (350 µs) were used. Collision cross-section (CCS) values were determined using multifield measurements and then drift tube entrance voltage was varied from 1074 V to 1674 V with 100 V increments (563 to 875V with 52V increments). Before sample introduction, ES tuning mix (Agilent Technologies) was measured as a quality control sample for CCS values.[4] Data was analyzed using MassHunter Qualitative Navigator (B.09.00) and MassHunter IM-MS Browser (B.08.00) from Agilent Technologies, USA. Theoretical CCS values were calculated with IMoSSuite 1.10,[5] and using experimental parameters (gas, temperature and pressure). Several theoretical approaches (project approximation (PA), trajectory method with Lennart-Jones parameters (TMLJ, TMLJQ), and elastic/diffuse hard sphere scattering (EHSS/DHSS)) were tested. Coordinates for CCS calculations were obtained from experimental single crystal XRD structures.

Single crystal X-ray diffraction

The experimental and refinement details for **2** and **3** are given below. Single crystal X-ray data was measured using a Rigaku SuperNova dual-source Oxford diffractometer equipped with an Atlas detector using mirror-monochromated Cu-*K*α (λ = 1.54184 Å) radiation. The data collection and reduction were performed using the program *CrysAlisPro*,[6] with an empirical absorption correction method using spherical harmonics correction applied to **2** and a numerical absorption correction based on gaussian integration over a multifaceted crystal model applied to **3**.[6] The structure was solved with intrinsic phasing (*ShelXT*)[7] and refined by full-matrix least squares on F^2 using the *Olex2* software,[8] which utilises the *ShelXL*-2015 module.[9] Anisotropic displacement parameters were assigned to non-H atoms. All hydrogen atoms were refined using riding models with U_{eq}(H) of 1.5U_{eq}(C) for sp^3 hybridized carbons and U_{eq}(H) of 1.2U_{eq}(C) for sp^2 hybridized carbons. The crystallographic data are available for free of charge downloading from the Cambridge Crystallographic Data Centre via www.ccdc.cam.ac.uk/datarequest/cif. CCDC-2192093 (**2**) and 2192095 (**3**)

As a result of supramolecular and highly porous nature of **2** and **3** both displayed rapid falloff of the reflection intensities, even with prolonged exposure times using Cu radiation, with no reflections whatsoever observed beyond 0.88 (**2**) and 0.87 (**3**) Å resolution. This necessitated moderate modelling using a range of restraints and constraints to account for the geometric (DFIX, DANG, FLAT) and thermal parameters (DELU, SIMU, RIGU, EADP) within parts of the structure, especially when disorder was found to be present as with the racemic $Co^{III}L_3$ nodes. The solvents present in **2** and **3** could not be modelled whatsoever and were accounted for using a Solvent Mask generated by the BYPASS module within Olex2,[8] which identified solvent accessible voids of 155117.0 $Å^3$ (and 21797.0 electrons per unit cell recovered) for **2** and 151818.6 $Å^3$ (with 39847.0 electrons per unit cell recovered) for **3**. Given the unidentifiable number and composition of solvents present, the formula weight, density etc. given does not include any correction for the missing solvates.

---

[4] a) V. Gabelica, A.A. Shvartsburg, C. Afonso, P. Barran, J.L.P. Benesch, C. Bleiholder, M.T. Bowers, A. Bilbao, M. F. Bush, J. L. Campbell, I.D.G. Campuzano, T. Causon, B.H. Clowers, C.S. Creaser, E. De Pauw, J. Far, F. Fernandez-Lima, J.C. Fjeldsted, K. Giles, M. Groessl, C. J. Hogan, S. Hann, H.I. Kim, R. Kurulugama, J. C. May, J. A. McLean, K. Pagel, K. Richardson, M.E. Ridgeway, F. Rosu, F. Sobott, K. Thalassinos, S.J. Valentine, T. Wyttenbach, Recommendations for Reporting Ion Mobility Mass Spectrometry Measurements. *Mass Spectrom. Rev.* **2019**, *38*, 291–320. b) S.M. Stow, T.J. Causon, X. Zheng, R.T. Kurulugama, T. Mairinger, J.C. May, E.E.Rennie, E.S. Baker, R.D. Smith, J.A. McLean, An Interlaboratory Evaluation of Drift Tube Ion Mobility–mass Spectrometry Collision Cross Section Measurements. *Anal. Chem.* **2017**, *89* , 9048–9055.

[5] C. Larriba-Andaluz, C.J. Jr. Hogan, Collision Cross Section Calculations for Polyatomic Ions Considering Rotating Diatomic/linear Gas Molecules. *J. Chem. Phys.* **2014**, *141*, 194107.

6 Rigaku Oxford Diffraction, 2018, *CrysAlisPro*, Rigaku Corporation, Oxford, UK.

7 G. M. Sheldrick, *SHELXT* - Integrated space-group and crystal-structure determination *Acta Crystallogr. Sect. A*, **2015**, *71*, 3–8.

8 O. V Dolomanov, L. J. Bourhis, R. J. Gildea, J. A. K. Howard, H. Puschmann, OLEX2: a complete structure solution, refinement and analysis program *J. Appl. Crystallogr.*, **2009**, *42*, 339–341.

9 G. M. Sheldrick Crystal structure refinement with SHELXL *Acta Crystallogr. Sect. C*, **2015**, *71*, 3–8.

Crystal data for **2**: $C_{624}H_{504}Co_{32}N_{48}O_{126}S_{24}$, M = 13345.65, red block, 0.23 x 0.26 x 0.28 mm^3, trigonal, space group *R*-3c, a = 37.1152(8) Å, c = 191.198(3) Å, V = 228095(11) $Å^3$, Z = 6, D_{calc} = 0.583 gcm^{-3}, F000 = 41040, μ = 3.23 mm^{-1}, T = 120.0(1) K, θ_{max} = 61.2°, 38980 total reflections, 19283 with $I_o > 2\sigma(I_o)$, R_{int} = 0.073, 38980 data, 1459 parameters, 352 restraints, GooF = 1.16, $R_1[I_o > 2\sigma(I_o)]$ = 0.137 and wR_2 = 0.378, 1.08 < dΔρ < -0.59 $eÅ^{-3}$, CCDC-2192093.

Crystal data for **3**: $C_{624}H_{504}Co_8N_{48}Ni_{24}O_{126}S_{24}$, M = 13340.38, red block, 0.24 x 0.24 x 0.38 mm^3, trigonal, space group *R*-3c, a = 36.9039(4) Å, c = 190.7619(15) Å, V = 224992(5) $Å^3$, Z = 6, D_{calc} = 0.591 gcm^{-3}, F000 = 41184, μ = 1.57 mm^{-1}, T = 120.0(1) K, θ_{max} = 62.0°, 39074 total reflections, 27425 with $I_o > 2\sigma(I_o)$, R_{int} = 0.067, 39074 data, 1489 parameters, 161 restraints, GooF = 1.10, $R_1[I_o > 2\sigma(I_o)]$ = 0.078 and wR_2 = 0.275, 0.45 < dΔρ < -0.43 $eÅ^{-3}$, CCDC- 2192095.

PXRD measurements

X-ray powder diffraction study of the samples was performed at X-ray structural analysis beamline (XSA) of Kurchatov Synchrotron Radiation Source. Monochromatic radiation with a wavelength of 0.8 Å (photon energy 15498 eV) was used. The sample was placed in a cryoloop of 300 μm in size and rotated around the horizontal axis during the measurement, which made it possible to average the diffraction patterns according to the orientations of the sample. Diffraction patterns were collected by the 2D Rayonix SX165 detector, which was located perpendicular to the SR beam at a distance of 120 mm, Debye−Scherrer (transmissional) geometry was used with a 400 μm beam size. The exposure time was 5 min. To calibrate the sample−detector distance we need a polycrystalline standard with a known position of the diffraction peaks; in this series of measurements LaB 6 (NIST SRM 660a) powder was used. The two-dimensional diffraction patterns obtained on the detector were further integrated to the standard form of the dependence of the intensity on the scattering angle I(2θ).

TGA measurements

A TG/DSC NETZSCH (Selb, Germany) STA449 F3 were used for the thermal analysis (thermogravimetry/differential scanning calorimetry) in which the variation of the sample mass as a function of temperature and the corresponding heats are recorded. An approximately 15 mg sample was placed in an Al crucible with a pre-hole on the lid and heated from 25 to 500°C.

Gas adsorption measurements

Surface Area and Porous Structure.

The porous structure was analyzed using the nitrogen adsorption technique on a Quantochrome's Autosorb iQ gas sorption analyzer at 77 K. Initially, the compound was activated under a dynamic vacuum at 180 °C for 6 h. The nitrogen adsorption−desorption isotherms were measured within the range of relative pressures from 10^{-6} to 0.995. The specific surface area was calculated from the data obtained using the conventional BET and DFT models (see details below).

Gases Sorption Experiments at 273 and 298 K.

Gases adsorption isotherm measurements were carried out volumetrically on Quantochrome's Autosorb iQ equiped with thermostat TERMEX Cryo-VT-12 to adjust temperature with 0.1 K accuracy. Adsorption−desorption isotherms were measured within the range of pressures of 1 to 800 torr. The database of the National Institute of Standards and Technology [Thermophysical Properties of Fluid Systems, Database of National Institute of Standards and Technology, NIST. http://webbook.nist.gov/chemistry/fluid/] was used as a source of p−V−T relations at experimental pressures and temperatures. (see details below)

Table S1: Crystallographic data for **2** and **3**, recorded at 120K.

	2	**3**
	[**1**-$Co^{II}_4(m_4\text{-}H_2O)]_6[(Co^{III}L)_2]_8$·XX DMF·XX H_2O	[**1**-$Ni^{II}_4(m_4\text{-}H_2O)]_6[(Co^{III}L)_2]_8$·XX DMF·XX H_2O
Formula	$C_{624}H_{504}Co_{32}N_{48}O_{126}S_{24}$ [+ solvent]	$C_{624}H_{504}Co_8Ni_{24}N4_8O_{126}S_{24}$ [+ solvent]
Molecular weight ($gmol^{-1}$)	13345.65	13340.38
Crystal system	trigonal	trigonal
Space group	*R*-3c	*R*-3c
a(Å)	37.1152(8)	36.9039(4)
b(Å)	37.1152(8)	36.9039(4)
c(Å)	191.198(3)	190.7619(15)
α(deg)	90	90
β(deg)	90	90
γ(deg)	120	120
V($Å^3$)	228095(11)	224992(5)
Z	6	6
Colour	red	red
Crystal dim (mm^3)	0.250 x 0.200 x 0.200	0.400 x 0.250 x 0.250
Dcalc (gcm^{-3})		
F(000)	41040	41184
μ (mm^{-1})	3.228	3.228
Wavelength (Å)	1.54184	1.54184
Temperature (K)	120	120
Number of data meas.	378068	356939
Number of data with I> 2σ(I)	38980	39074
R (%)	0.1365	0.0778
Rw (%)	0.1674	0.0941
GOF	1.162	1.096
Largest peak in final difference ($eÅ^{-3}$)	1.078	0.453

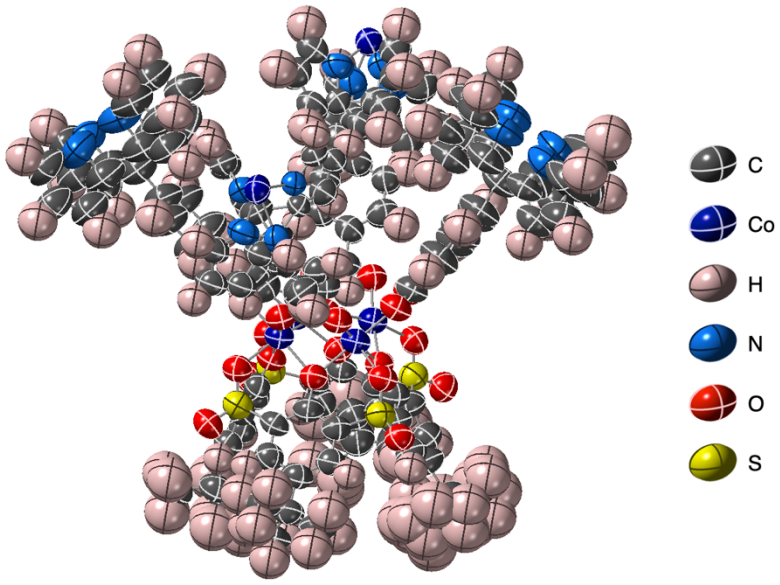

Figure S1. For **2**, ORTEP view of the asymmetric unit, obtained from X-ray diffraction data.

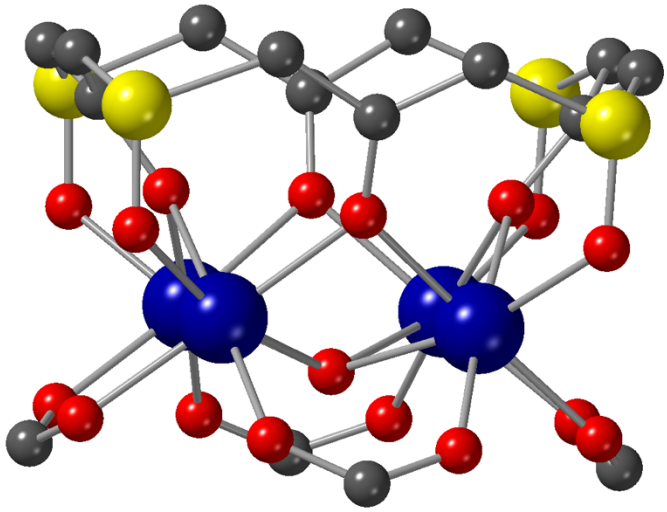

Figure S2. For **2**, view of the surrounding of the M^{II} (Co or Ni) cations in the [**1**-$M^{II}_4(m_4\text{-}H_2O)]^{4+}$ units and their coordination spheres, obtained from X-ray diffraction data.

IR spectroscopy

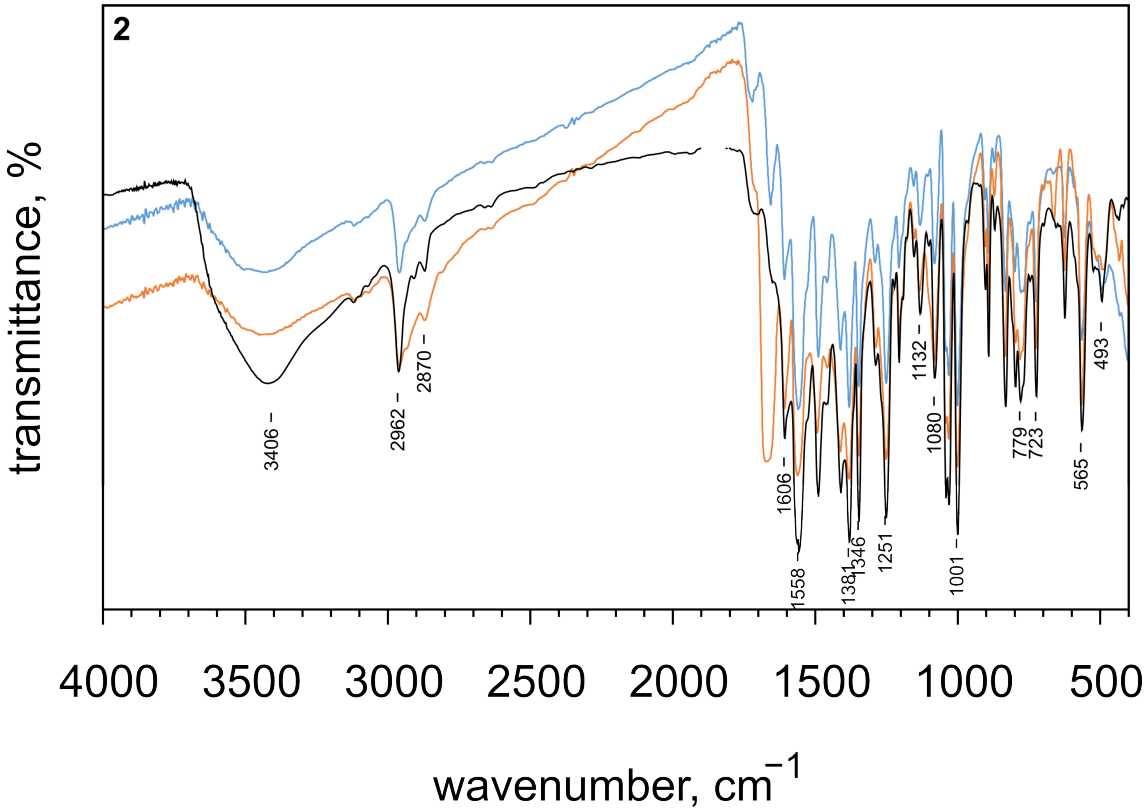

Figure S3a. FT-IR spectrum for compound **2**: as synthesized (blue), activated (red), after gases adsorption (black).

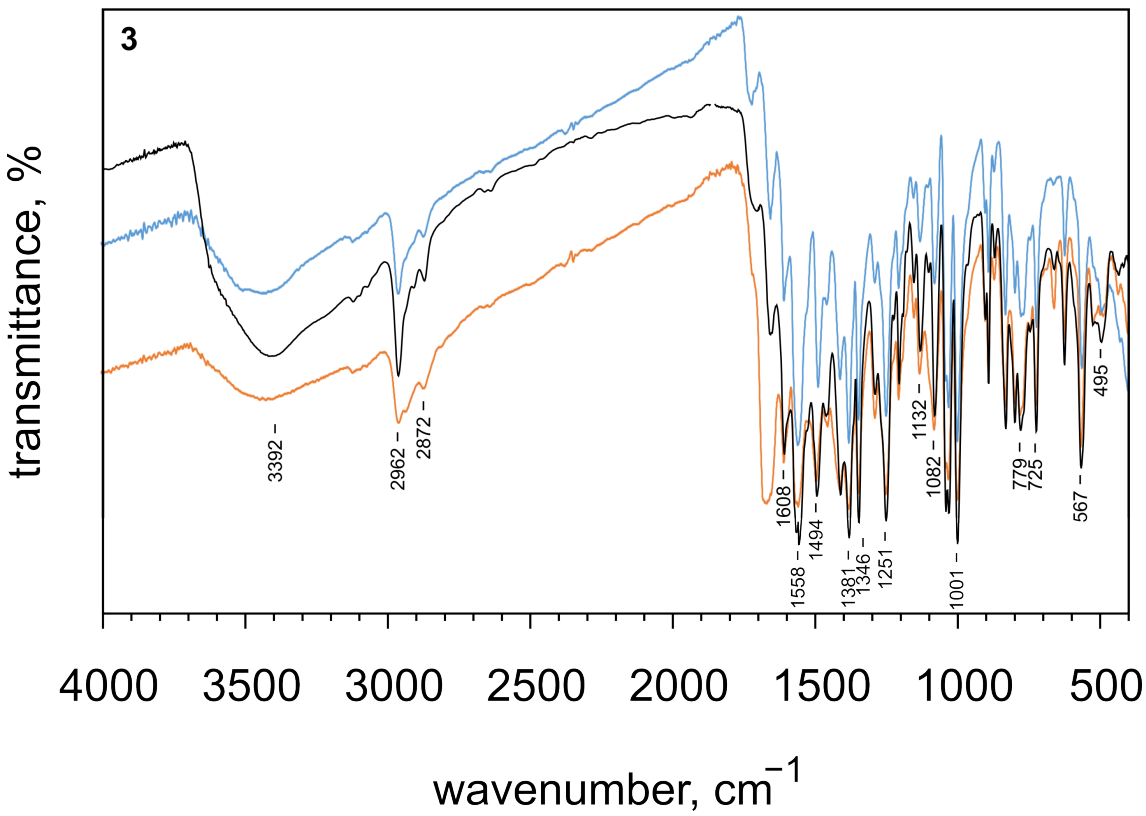

Figure S3b. FT-IR spectrum for compound **3**: as synthesized (blue), activated (red), after gases adsorption (black).

ESI-MS and IM-MS data for 2 and 3.

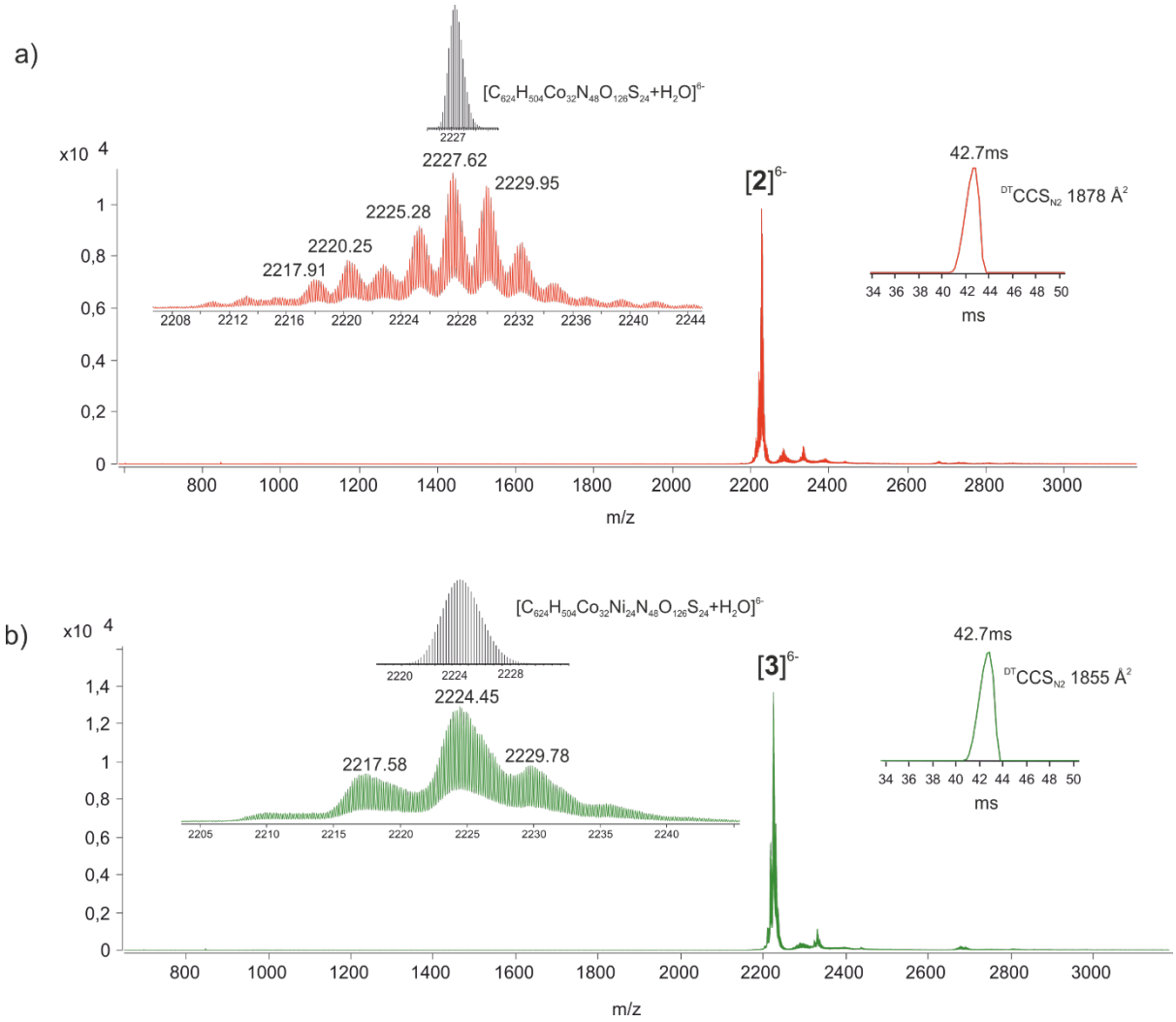

Figure S4. (-)ESI-MS spectra for cages a) **2** and b) **3**. Insets on left show zoomed view for base peak and peaks originating from different adducts. Comparison to theoretical isotopic distributions are shown above inset with black line. Insets on right show ion mobility arrival time distributions, drift times and collision cross section values (drift tube IM, N_2) for the main peaks. Theoretical $^{EHSS}CCS_{N2}$ values for empty cages is 1834.3 Å^2 for both [**2**]$^{6-}$ and [**3**]$^{6-}$.

TGA analysis

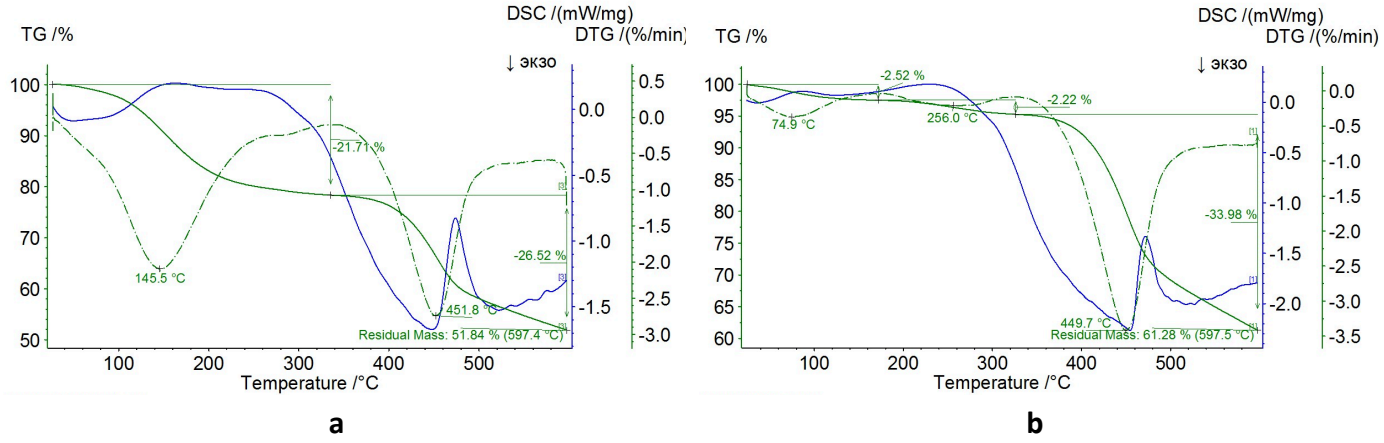

Figure S5. TGA/DSC traces of **2** between RT and 600°C for a) the as synthesized compound b) the activated compound.

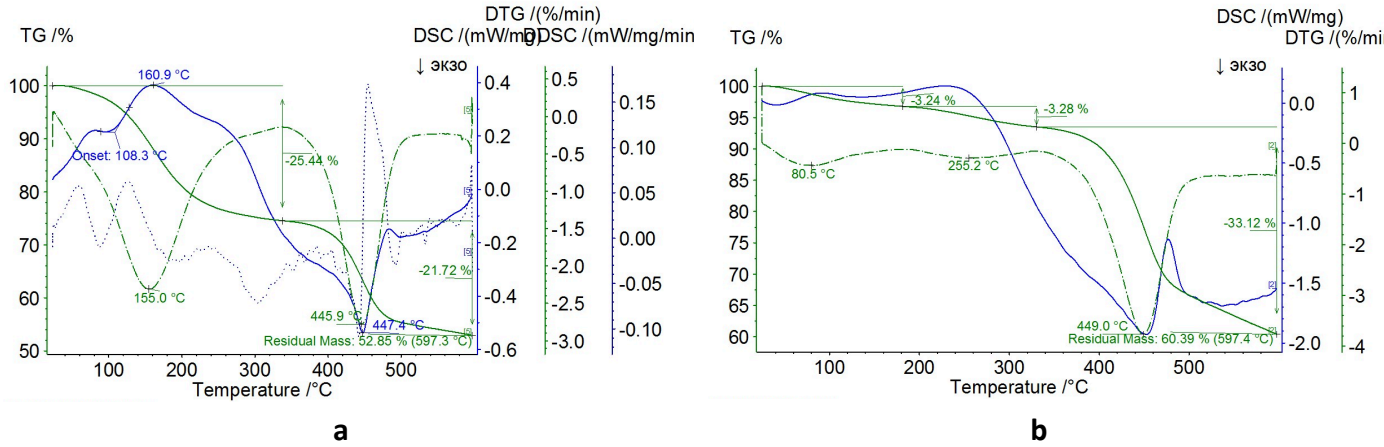

Figure S6. TGA/DSC traces of **3** between RT and 600°C for a) the as synthesized compound b) the activated compound.

XRPD diagrams

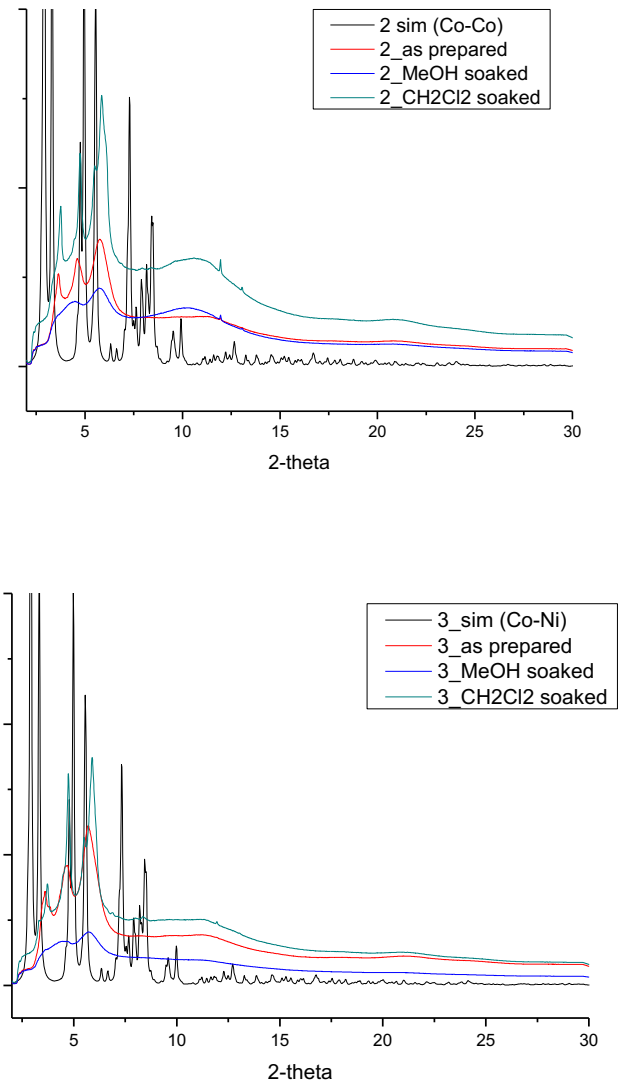

Figure S7. The powder X-Ray diffraction (PXRD) studies for freshly prepared, soaked in MeOH and CH2Cl2 powdered samples of **2** (a) and **3** (b).

Gas adsorption properties

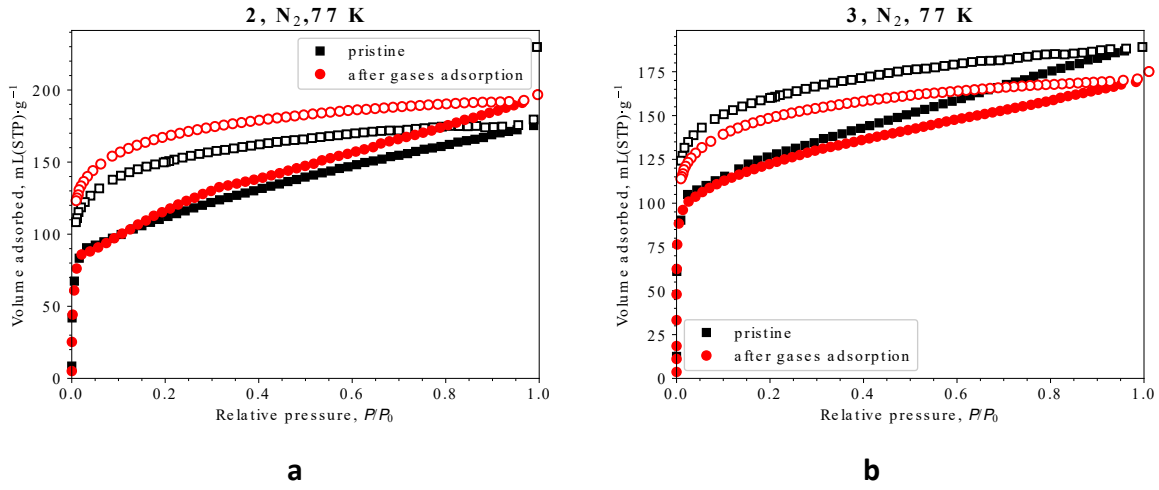

Figure S8. Nitrogen adsorption-desorption isotherms at 77 K (filled symbols for adsorption, hollow ones for desorption) for **2** (a) and **3** (b).

Table S2. Characteristic parameters for **2** and **3**

Sample	Specific surface area / $m^2 \cdot g^{-1}$			V_{pore} / $cm^3 \cdot g^{-1}$		$V_{ads}(N_2)^a$ / $cm^3(STP) \cdot g^{-1}$
	Langmuir	BET	DFT	Total[a]	DFT	
2	461.7	416.9	323.4	0.293	0.281	189.8
2 after gases adsorption	510.2	396.2	327.9	0.267	0.253	172.4
3	505.8	445.2	476.6	0.259	0.244	167.5
3 after gases adsorption	513.3	454.1	396.9	0.289	0.272	186.9

[a] measured at $P/P_0 = 0.95$.

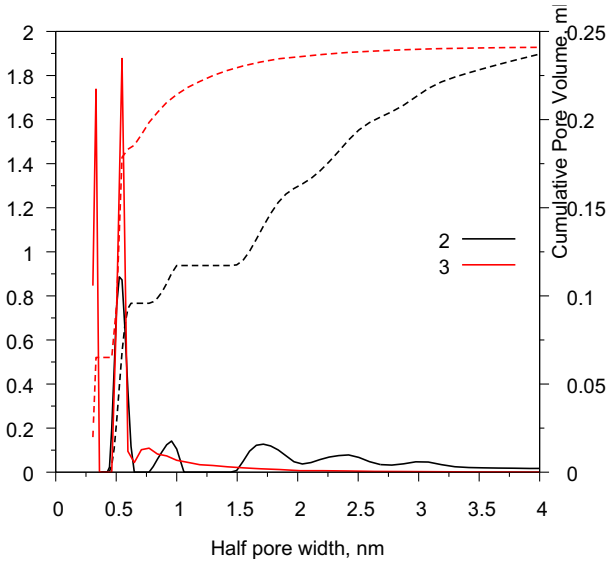

Figure S9. Calculated pore size distributions (solid lines) and cumulative pore volumes (dashed lines) for **2** and **3**.

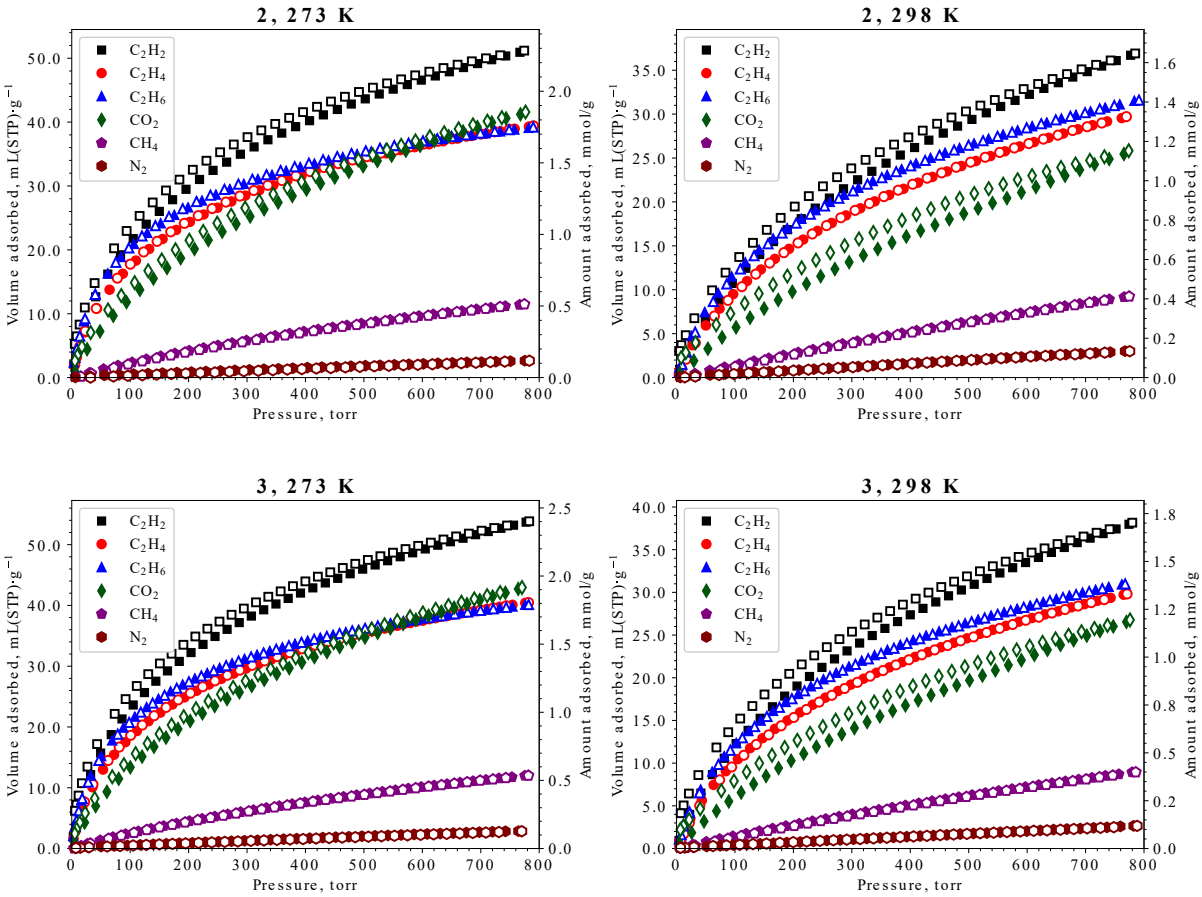

Figure S10. Gas adsorption (filled symbols) -desorption (hollow symbols) isotherms for **2** (top) and **3** (bottom) at 273 K (left) and 298 K (right) between 0 and 800 torr (1,07 bar).

Fit of adsorption isotherms for N_2, CO_2, CH_4, C_2H_2, C_2H_4 and C_2H_6

For IAST calculations isotherms of CO_2, C_2H_2, C_2H_4, C_2H_6 adsorption were fitted by Langmuir-Freundlich equation $n = \frac{wbp^{1/t}}{1+bp^{1/t}}$ or (in case of CO_2 adsorption at 298 K) by the sum of Henry and Langmuir equation $n = kp + \frac{wbp}{1+bp}$.

For IAST calculations isotherms of CH_4 and N_2 adsorption were fitted by Langmuir equation $n = \frac{wbp}{1+bp}$.

Fittings were performed for isotherms in mL/g–torr units, so parameters are in the corresponding units.

Final sets of parameters are summarized in Table S3. Measured isotherms and fitted curves are shown in Figure S10 for comparison of coincidence.

Table S3. Fitted parameters for adsorption isotherms on compounds of **2** and **3** at 273 K and 298 K

Gas	273 K	298 K
	2	
C_2H_2	Langmuir-Freundlich *w* = 97.2963 ± 2.054 (2.111%) *b* = 0.0122422± 0.0002126 (1.737%) *t* = 1.4802± 0.01815 (1.226%)	Langmuir-Freundlich *w* = 94.4424 ± 3.005 (3.182%) *b* = 0.00391939 ± 5.759e-05 (1.469%) *t* = 1.30981 ± 0.01473 (1.125%)
C_2H_4	Langmuir-Freundlich *w* = 62.0336 ± 0.7408 (1.194%) *b* = 0.013891 ± 0.0002846 (2.049%) *t* = 1.38354 ± 0.01392 (1.006%)	Langmuir-Freundlich *w* = 62.72 ± 1.295(2.064%) *b* = 0.00494205 ± 8.576e-05 (1.735%) *t* = 1.27827 ± 0.01259(0.9852%)
C_2H_6	Langmuir-Freundlich *w* = 55.0052 ± 0.4667 (0.8485%) *b* = 0.0235891± 0.0004647 (1.97%) *t* = 1.43608 ± 0.01374(0.9568%)	Langmuir-Freundlich *w* = 57.2299 ± 1.093(1.911%) *b* = 0.00832491 ± 0.0001917 (2.302%) *t* = 1.33754 ± 0.01607(1.201%)
CO_2	Langmuir-Freundlich *w* = 101.248 ± 2.106(2.08%) *b* = 0.00371982 ± 4.284e-05 (1.152%) *t* = 1.27422 ± 0.01001(0.7857%)	Henry + Langmuir *k* = 0.0189987± 0.0003941 (2.074%) *w* = 14.9707 ± 0.578(3.861%) *b* = 0.0033817± 0.0001531 (4.528%)
CH_4	Langmuir *w* = 29.2626 ± 0.2863 (0.9785%) *b* = 0.000827783± 1.177e-05 (1.422%)	Langmuir *w* = 52.1426 ± 0.3686 (0.7069%) *b* = 0.000278263± 2.287e-06 (0.8218%)
N_2	Langmuir *w* = 9.62073 ± 0.5417 (5.63%) *b* = 0.00048082 ± 3.456e-05 (7.188%)	Langmuir *w* = 41.1654 ± 5.363 (13.03%) *b* = 0.000102284 ± 1.414e-05 (13.83%)
	3	
C_2H_2	Langmuir-Freundlich w = 100.559 ± 1.8 (1.79%) b = 0.0140435± 0.0002067 (1.472%) t = 1.51508 ± 0.01628(1.075%)	Langmuir-Freundlich w = 91.0126 ± 2.312(2.541%) b = 0.00476134 ± 6.441e-05 (1.353%) t = 1.32911 ± 0.01322(0.9943%)
C_2H_4	Langmuir-Freundlich w = 63.5447 ± 0.6161 (0.9696%) b = 0.0148832± 0.0002413 (1.621%) t = 1.39885 ± 0.01147(0.8197%)	Langmuir-Freundlich w = 60.1993 ± 0.9727 (1.616%) b = 0.00567625 ± 8.538e-05 (1.504%) t = 1.2913± 0.01072(0.8303%)
C_2H_6	w = 56.5787 ± 0.4088 (0.7225%) b = 0.0241991± 0.0003904 (1.613%) t = 1.44569 ± 0.01161(0.8029%)	w = 53.6991 ± 0.7455 (1.388%) b = 0.00904394 ± 0.000173 (1.913%) t = 1.32589 ± 0.01258(0.9484%)
CO_2	Langmuir-Freundlich w = 101.546 ± 1.867(1.838%) b = 0.00430711 ± 4.539e-05 (1.054%) t = 1.29642 ± 0.009412 (0.726%)	Henry + Langmuir k = 0.0198953± 0.0003584 (1.801%) w = 15.0611 ± 0.5012 (3.327%) b = 0.00373415 ± 0.0001524 (4.081%)
CH_4	Langmuir w = 28.5561 ± 0.3721 (1.303%) b = 0.000920656± 1.801e-05 (1.957%)	Langmuir w = 37.8363 ± 0.5196 (1.373%) b = 0.000394262± 6.656e-06 (1.688%)
N_2	Langmuir w = 11.9083 ± 0.6685 (5.614%) b = 0.000414686 ± 2.878e-05 (6.94%)	Langmuir w = 26.0459 ± 2.811 (10.79%) b = 0.000143507 ± 1.683e-05 (11.73%)

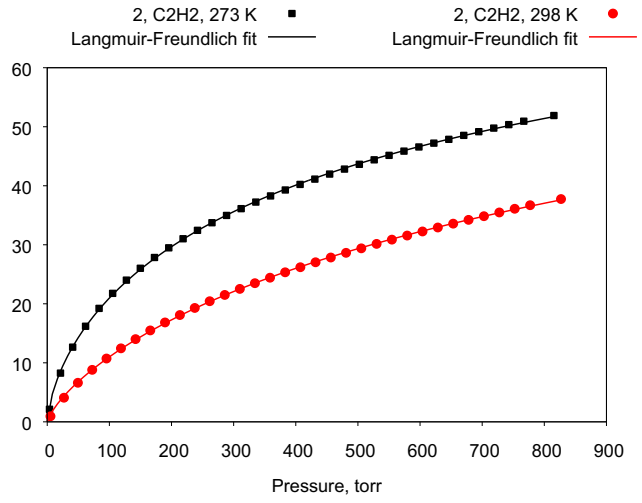
2, C2H2, 273 K
Langmuir-Freundlich fit
2, C2H2, 298 K
Langmuir-Freundlich fit
60
50
40
30
20
10
0
0
100
200
300
400
500
600
700
800
900
Pressure, torr

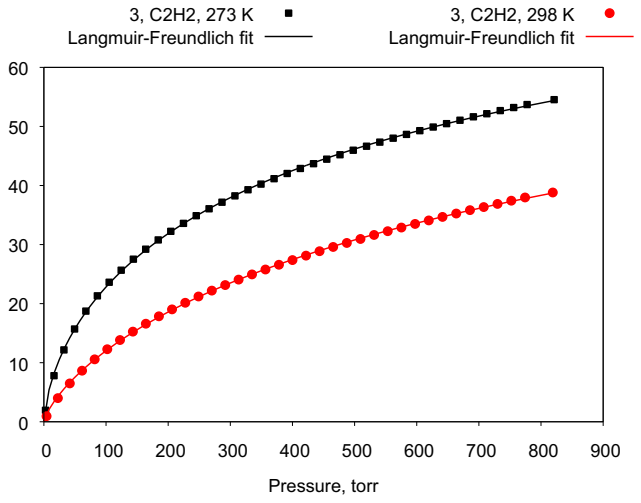
3, C2H2, 273 K
Langmuir-Freundlich fit
3, C2H2, 298 K
Langmuir-Freundlich fit
60
50
40
30
20
10
0
0
100
200
300
400
500
600
700
800
900
Pressure, torr

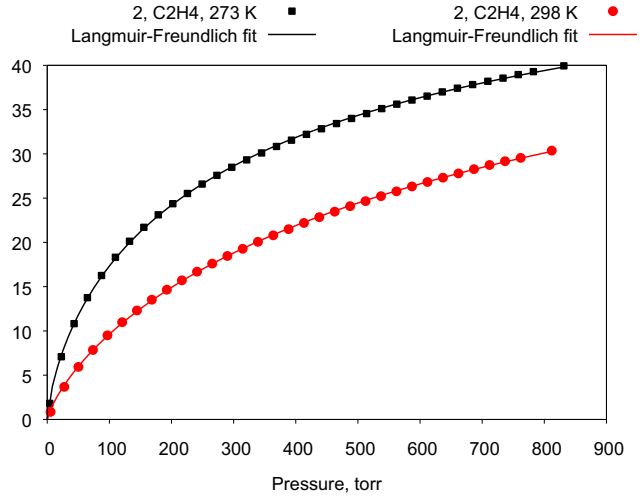
2, C2H4, 273 K
Langmuir-Freundlich fit
2, C2H4, 298 K
Langmuir-Freundlich fit
40
35
30
25
20
15
10
5
0
0
100
200
300
400
500
600
700
800
900
Pressure, torr

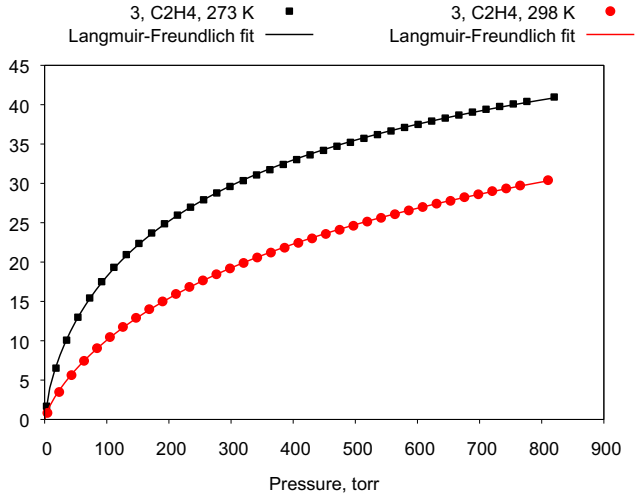
3, C2H4, 273 K
Langmuir-Freundlich fit
3, C2H4, 298 K
Langmuir-Freundlich fit
45
40
35
30
25
20
15
10
5
0
0
100
200
300
400
500
600
700
800
900
Pressure, torr

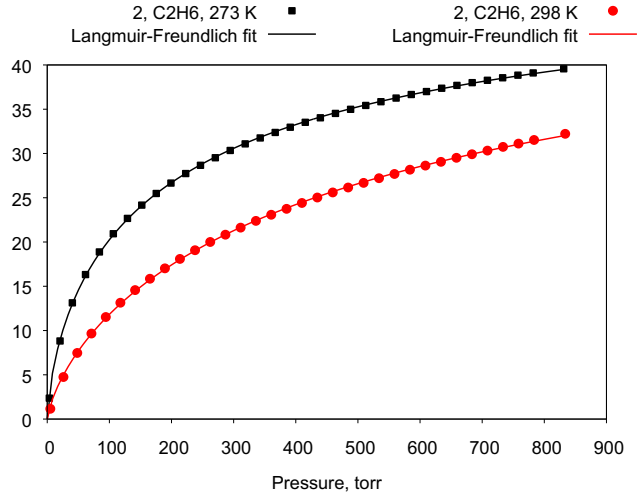
2, C2H6, 273 K
Langmuir-Freundlich fit
2, C2H6, 298 K
Langmuir-Freundlich fit
40
35
30
25
20
15
10
5
0
0
100
200
300
400
500
600
700
800
900
Pressure, torr

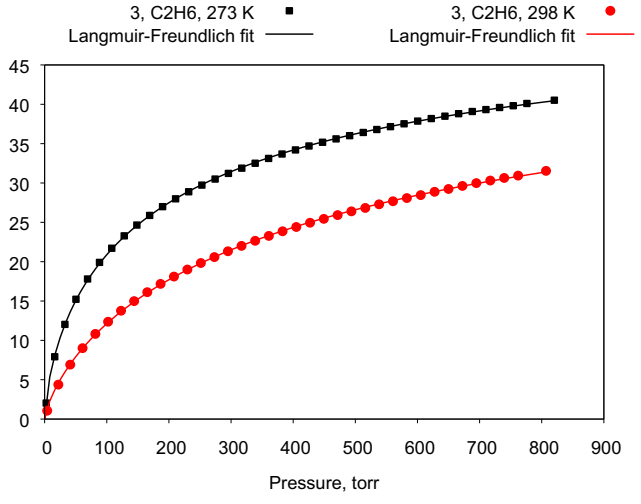
3, C2H6, 273 K
Langmuir-Freundlich fit
3, C2H6, 298 K
Langmuir-Freundlich fit
45
40
35
30
25
20
15
10
5
0
0
100
200
300
400
500
600
700
800
900
Pressure, torr

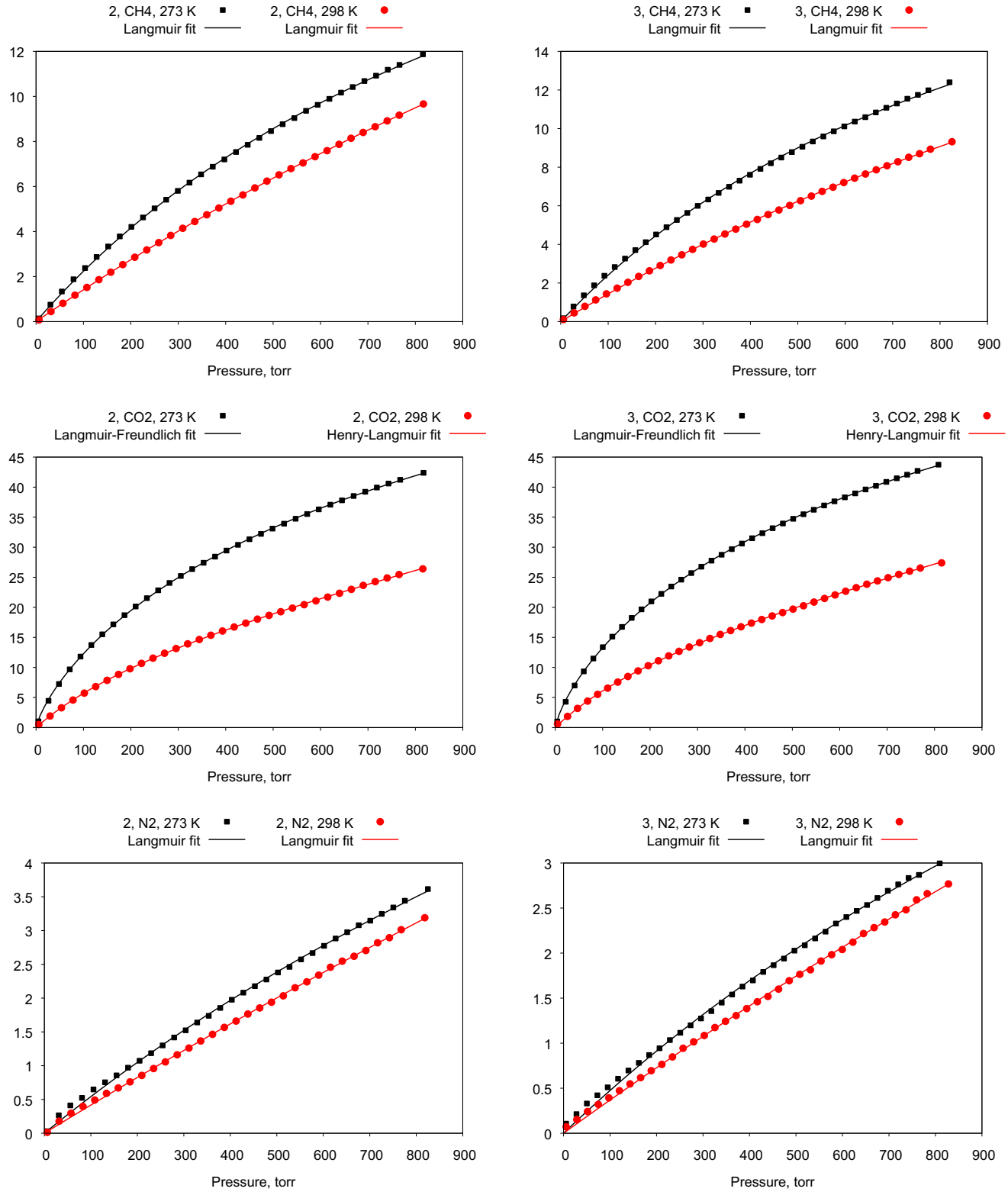

Figure S11. Fits of isotherms by appropriate models.

Table S4. Gas uptakes on **2** and **3** series at 273 K and 298 K at 1 bar.

Gas	273 K			298 K		
	mL(STP)/g	mmol/g	wt. %	mL(STP)/g	mmol/g	wt. %
2						
C_2H_2	50.5	2.25	5.5	36.0	1.61	4.0
C_2H_4	38.8	1.73	4.6	29.4	1.31	3.5
C_2H_6	38.8	1.73	4.9	31.0	1.38	4.0
CO_2	40.8	1.82	7.4	25.1	1.12	4.7
CH_4	11.3	0.50	0.8	9.0	0.40	0.6
N_2	3.4	0.15	0.5	2.9	0.13	0.4
3						
C_2H_2	53.1	2.37	5.8	37.4	1.67	4.2
C_2H_4	40.0	1.79	4.8	29.5	1.32	3.6
C_2H_6	39.8	1.77	5.1	30.8	1.37	4.0
CO_2	42.3	1.89	7.7	26.1	1.16	4.9
CH_4	11.7	0.52	0.8	8.6	0.39	0.6
N_2	2.8	0.13	0.4	2.5	0.11	0.3

Isotherms fit by virial equation

Gas adsorption isotherms at 273 K and 298 K were fitted by virial equation (S1) in order to calculate Henry constants and isosteric heats of adsorption.

$$lnp = lnn + \frac{1}{T}\sum_i A_i \cdot n^i + \sum_j B_j \cdot n^j \quad \text{(S1)}$$

Virial coefficients are summarized in Table S5, whereas fit plot are shown in Figure S11.

Table S5. Virial coefficients A_i and B_j for gas adsorption isotherms at 273 K and 298 K on **2** and **3**.

Gas	Coefficients	
	2	**3**
C_2H_2	A_0 = −3531.3 ± 36.98 (1.047%) A_1 = 248.258 ± 2.631 (1.06%) B_0 = 10.0926 ± 0.1237 (1.226%)	A_0 = −3741.53 ± 37.08 (0.9909%) A_1 = 254.844 ± 2.505 (0.9832%) B_0 = 10.6634 ± 0.1239 (1.162%)
C_2H_4	A_0 = −3298.93 ± 24.89 (0.7546%) A_1 = 337.79 ± 2.315 (0.6854%) B_0 = 9.36013 ± 0.08321 (0.8889%)	A_0 = −3537.13 ± 22.44 (0.6344%) A_1 = 347.085 ± 2.035 (0.5864%) B_0 = 10.0898 ± 0.07492 (0.7425%)
C_2H_6	A_0 = −3450.41 ± 43.52 (1.261%) A_1 = 413.873 ± 4.241 (1.025%) B_0 = 9.38848 ± 0.1448 (1.543%)	A_0 = −3723.56 ± 29.67 (0.7967%) A_1 = 419.06 ± 2.797 (0.6674%) B_0 = 10.2747 ± 0.09859 (0.9596%)
CO_2	A_0 = −3365.16 ± 42.58 (1.265%) A_1 = 191.612 ± 3.539 (1.847%) B_0 = 10.4926 ± 0.1433 (1.365%)	A_0 = −3497.17 ± 65.48 (1.872%) A_1 = 201.389 ± 5.285 (2.624%) B_0 = 10.833 ± 0.2201 (2.032%)
CH_4	A_0 = −1406.62 ± 43.83 (3.116%) A_1 = 222.827 ± 12.99 (5.829%) B_0 = 5.38465 ± 0.1504 (2.793%)	A_0 = −1781.33 ± 28.14 (1.58%) A_1 = 315.761 ± 8.088 (2.562%) B_0 = 6.56696 ± 0.09607 (1.463%)
N_2	A_0 = −839.886 ± 105.9 (12.61%) A_1 = 479.414 ± 104.1 (21.72%) B_0 = 4.70149 ± 0.3666 (7.798%)	A_0 = −868.507 ± 158.7 (18.27%) A_1 = 1322.24 ± 186.6 (14.11%) B_0 = 4.70937 ± 0.5502 (11.68%)

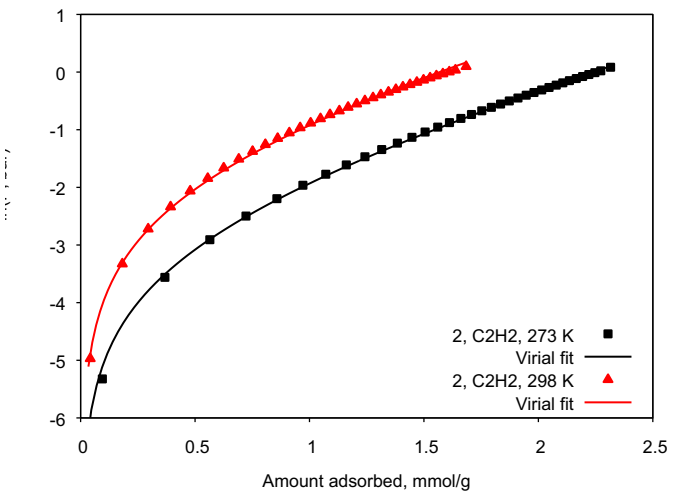

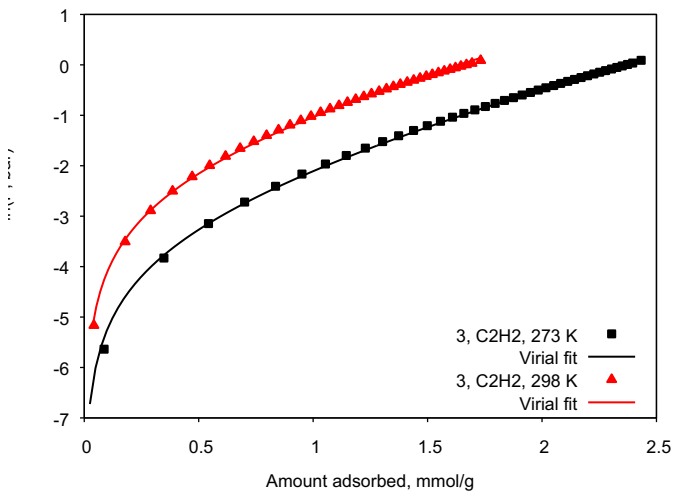

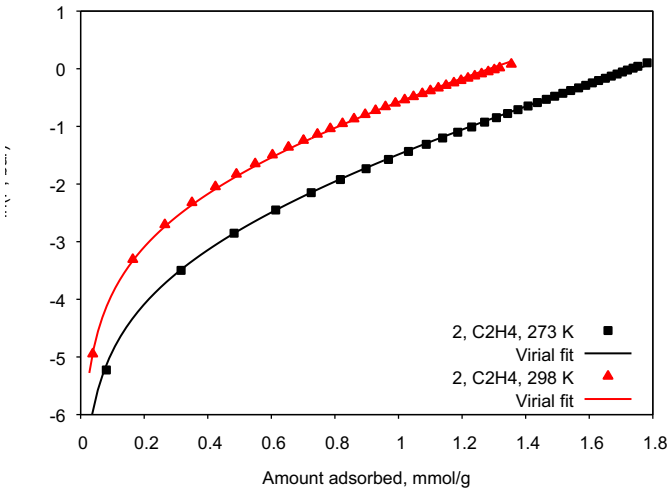
2, C2H4, 273 K
Virial fit
2, C2H4, 298 K
Virial fit
Amount adsorbed, mmol/g

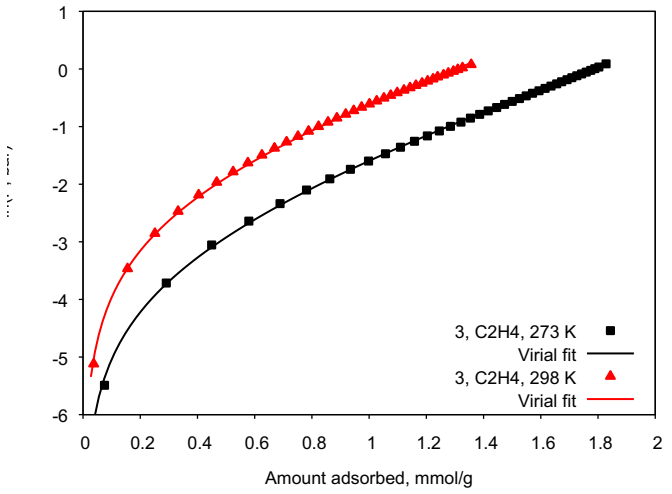
3, C2H4, 273 K
Virial fit
3, C2H4, 298 K
Virial fit
Amount adsorbed, mmol/g

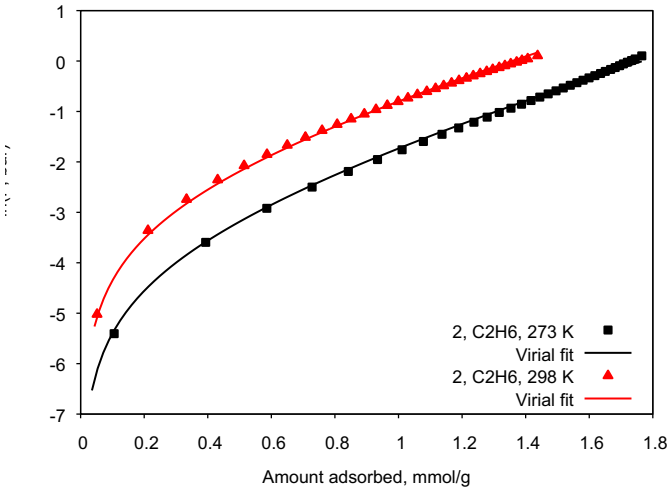
2, C2H6, 273 K
Virial fit
2, C2H6, 298 K
Virial fit
Amount adsorbed, mmol/g

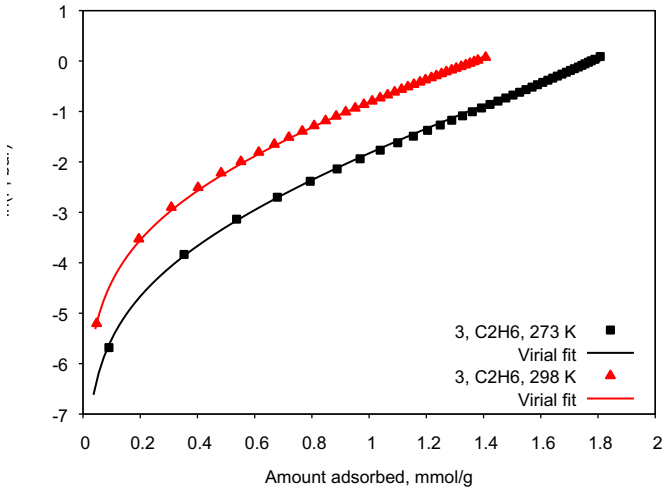
3, C2H6, 273 K
Virial fit
3, C2H6, 298 K
Virial fit
Amount adsorbed, mmol/g

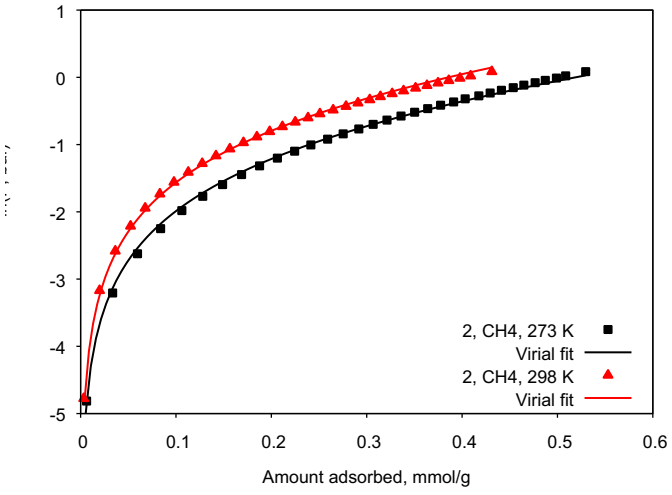
2, CH4, 273 K
Virial fit
2, CH4, 298 K
Virial fit
Amount adsorbed, mmol/g

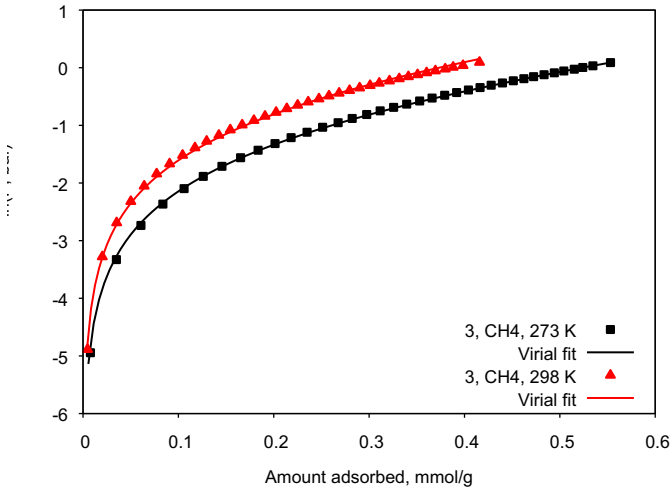
3, CH4, 273 K
Virial fit
3, CH4, 298 K
Virial fit
Amount adsorbed, mmol/g

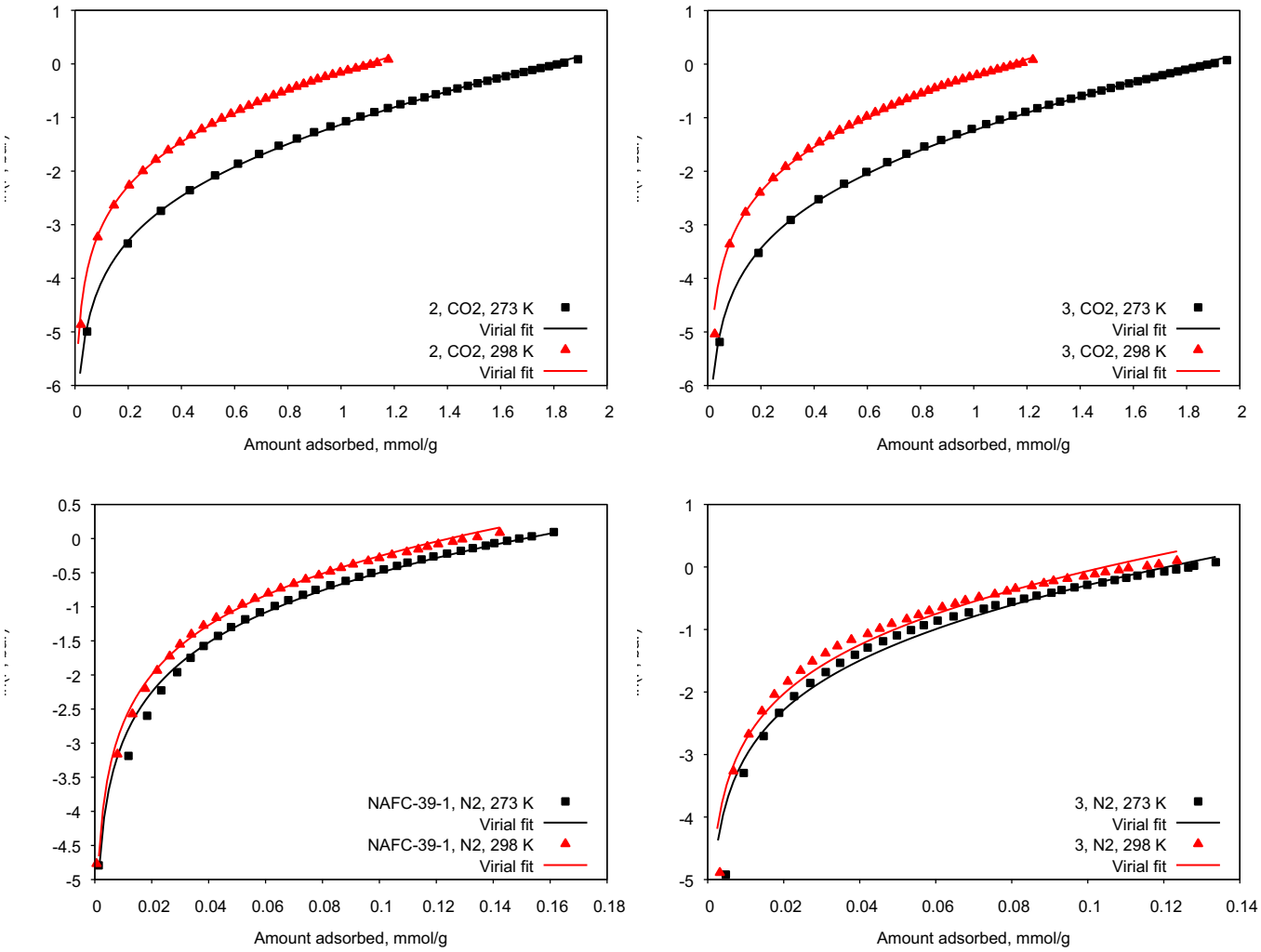

Fig. S12. Fits of isotherms by virial equations for **2** and **3**.

Henry constants

Henry constants were calculated using virial coefficients by equation (S2):

$$K_h = exp\left[\frac{-A_0}{T} - B_0\right] \quad \text{(S2)}$$

Table S6. Henry constants for gas adsorption for **2** and **3** in mmol·g^{-1}·bar^{-1} at 273 K and 298 K.

Gas\Temperature	273 K	298 K
2		
C_2H_2	17.04	5.76
C_2H_4	15.14	5.50
C_2H_6	25.62	8.88
CO_2	6.22	2.21
CH_4	0.79	0.51
N_2	0.20	0.15
3		
C_2H_2	20.79	6.59
C_2H_4	17.46	5.89
C_2H_6	28.71	9.15
CO_2	7.17	2.45
CH_4	0.956	0.553
N_2	0.217	0.166

Heats of adsorption

Isosteric heats of adsorption were calculated using virial coefficients by equation (S3):

$$\Delta H^{\circ} = R \cdot \sum_{i} A_i \cdot n^i \qquad \text{(S3)}$$

Table S7. Zero coverage heats of adsorption for **2** and **3** in kJmol^{-1}.

Gas	$Q_{st}(0)$, kJ/mol
2	
C_2H_2	29.4
C_2H_4	27.4
C_2H_6	28.7
CO_2	28.0
CH_4	11.7
N_2	7.0
3	
C_2H_2	31.1
C_2H_4	29.4
C_2H_6	31.0
CO_2	29.1
CH_4	14.8
N_2	7.2

Isosteric heats of adsorption were calculated by means of virial equation (S1) and equation (S2).

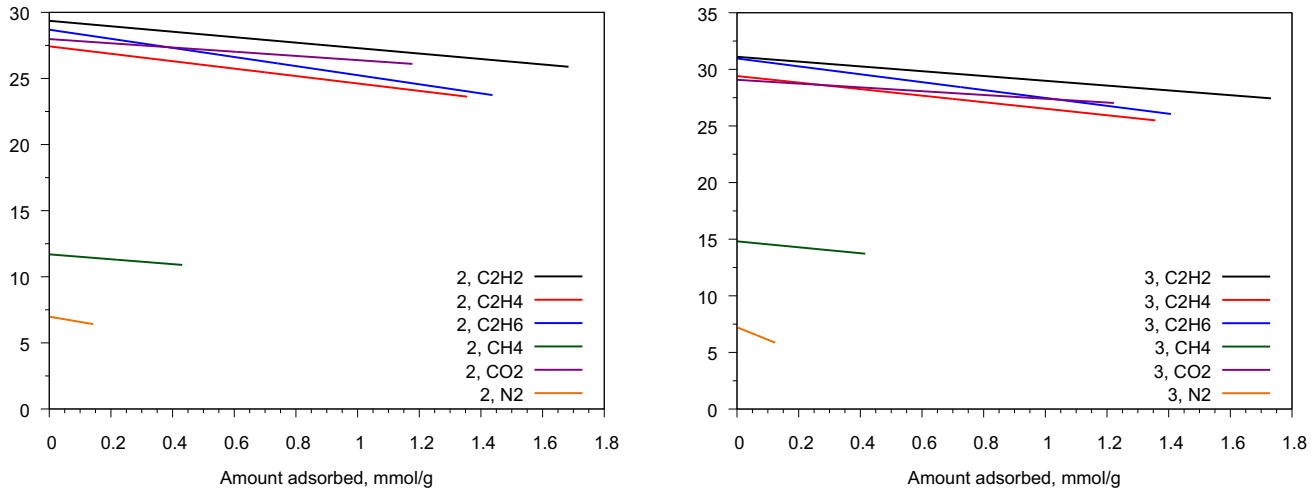

Figure S13. Graphs of isosteric heats of adsorption of all measured gases on **2** and **3**.

Selectivity of adsorption

Selectivity factors for separation of selected binary gas mixtures have been evaluated using three different methods: i) as ratio of amount adsorbed; ii) as ratio of corresponding Henry constants; and iii) by Ideal Adsorbed Solution Theory (IAST)[10] calculations which possess to estimate selectivity factors at different gas mixture compositions and total pressures. The relationship between P, y_i and x_i (P — the total pressure of the gas phase, y_i — mole fraction of the i-component in gas phase, x_i — mole fraction of the i-component in absorbed state) is defined according to

$$\int_{p=0}^{p=\frac{Py_1}{x_1}} n_1(p)d\ln p = \int_{p=0}^{p=\frac{Py_2}{x_2}} n_2(p)d\ln p$$

And the selectivity factors were determined as:

$$S = \frac{y_2/x_2}{y_1/x_1} = \frac{x_1(1-y_1)}{y_1(1-x_1)}$$

The results are summarized in Table S8 and in Figures below.

Table S8. For **2** and **3**, at T=273 and 298K, selectivity factors for separation of equimolar binary gas mixtures evaluated by different approach: i) as ratio of amount adsorbed V_1/V_2; ii) as ratio of corresponding Henry constants and iii) by Ideal Adsorbed Solution Theory (IAST) calculations.

Mixture	273 K			298 K		
	V_1/V_2	K_{H1}/K_{H2}	IAST	V_1/V_2	K_{H1}/K_{H2}	IAST
2						
C_2H_2/C_2H_4	1.3	1.1	1.8	1.2	1.0	1.3
C_2H_2/CO_2	1.2	2.7	5.7	1.4	2.6	5.4
C_2H_2/CH_4	4.5	21.6	18.3	4.0	11.3	11.9
C_2H_6/CH_4	3.4	32.4	18.7	3.4	17.4	13.8
CO_2/CH_4	3.6	7.9	8.9	2.8	4.3	2.7
CO_2/N_2	12.0	31.1	19.3	8.7	14.7	12.5
3						
C_2H_2/C_2H_4	1.3	1.2	2.0	1.3	1.1	1.5
C_2H_2/CO_2	1.3	2.9	6.1	1.4	2.7	5.7
C_2H_2/CH_4	4.5	21.7	19.5	4.3	11.9	12.8
C_2H_6/CH_4	3.4	30.0	18.5	3.6	16.5	13.6
CO_2/CH_4	3.6	7.5	9.4	3.0	4.4	2.8
CO_2/N_2	15.1	33.0	22.5	10.4	14.8	5.7

10 L. Myers, J. M. Prausnitz Thermodynamics of mixed-gas adsorption, *AIChE J*. **1965**, *11*, 121-127.

Results of IAST calculations

The graphs below show the results of IAST calculation: i) predictions of adsorption equilibrium by IAST at total pressure in gas phase of 1 bar: dependencies of mole fraction of gas adsorbed on its mole fraction in gas phase (solid lines, left column) and dependencies of selectivity factors on gas phase composition (dashed lines, left column); ii) dependencies of selectivity factors on total pressure of equimolar binary mixture (right column).

All calculations were performed based on one-component adsorption isotherms in order to evaluate the most efficient systems for selective adsorption. Results show moderate-to-high selectivity in adsorption of binary mixtures on both **2** and **3**, therefore both compounds are good candidates for further studies in separation of industrially important gas mixtures.

Some of the results obtained are not discussed in the main text due to not high significance of values got. Nevertheless, we decided to present all data obtained in order to provide full information about compounds obtained for specialists and interested readers.

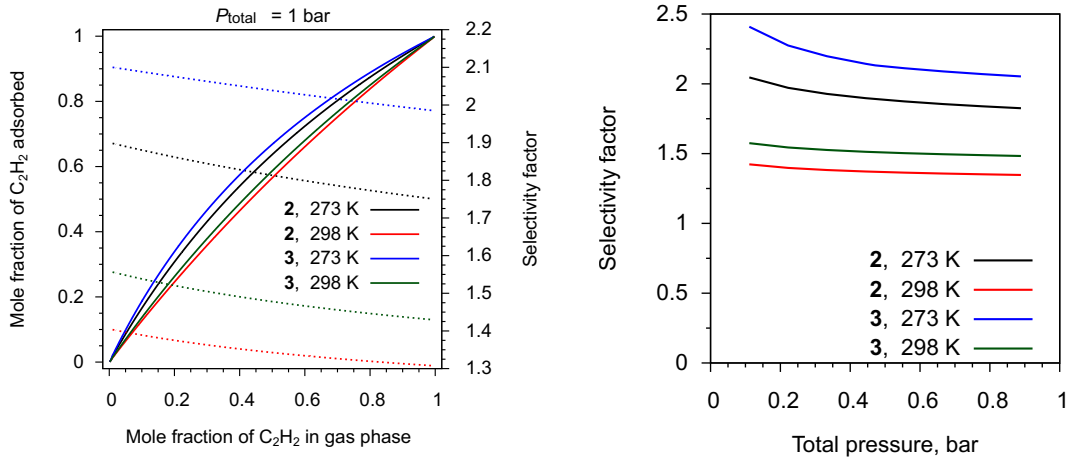

Figure S14. For binary **C_2H_2/C_2H_4** mixture: left, prediction of adsorption equilibrium by IAST (solid lines) and dependence of selectivity factors on gas phase composition (dashed lines) at total pressure 1 bar for **2** and **3**; right, graphs of adsorption selectivity dependence on the total pressure of gases mixture for **2** and **3**.

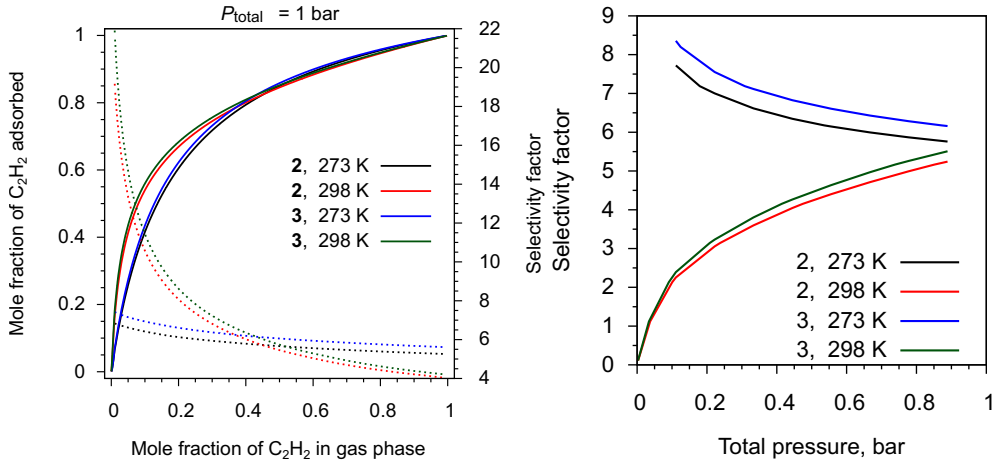

Figure S15. For binary **C_2H_2/CO_2** mixture: left, prediction of adsorption equilibrium by IAST (solid lines) and dependence of selectivity factors on gas phase composition (dashed lines) at total pressure 1 bar for **2** and **3**; right, graphs of adsorption selectivity dependence on the total pressure of gases mixture for **2** and **3**.

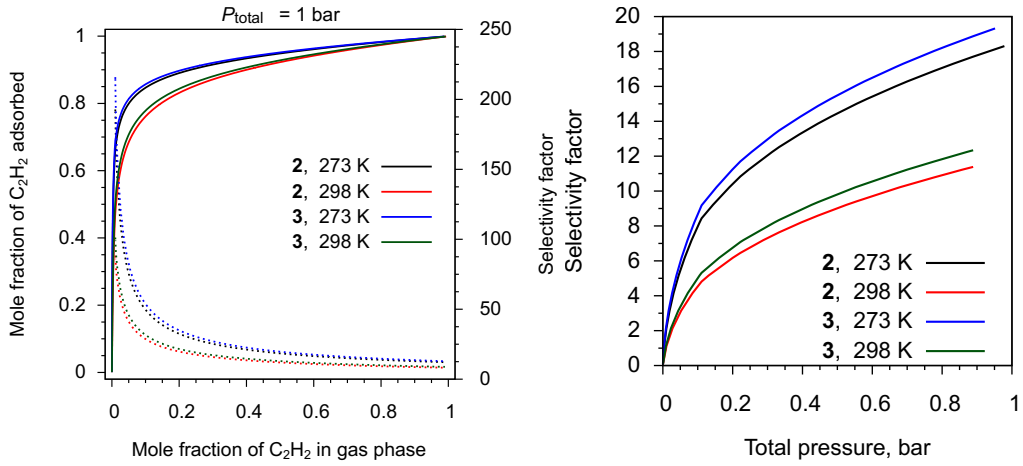

Figure S16. For binary C_2H_2/CH_4 mixture: left, prediction of adsorption equilibrium by IAST (solid lines) and dependence of selectivity factors on gas phase composition (dashed lines) at total pressure 1 bar for **2** and **3**; right, graphs of adsorption selectivity dependence on the total pressure of gases mixture for **2** and **3**.

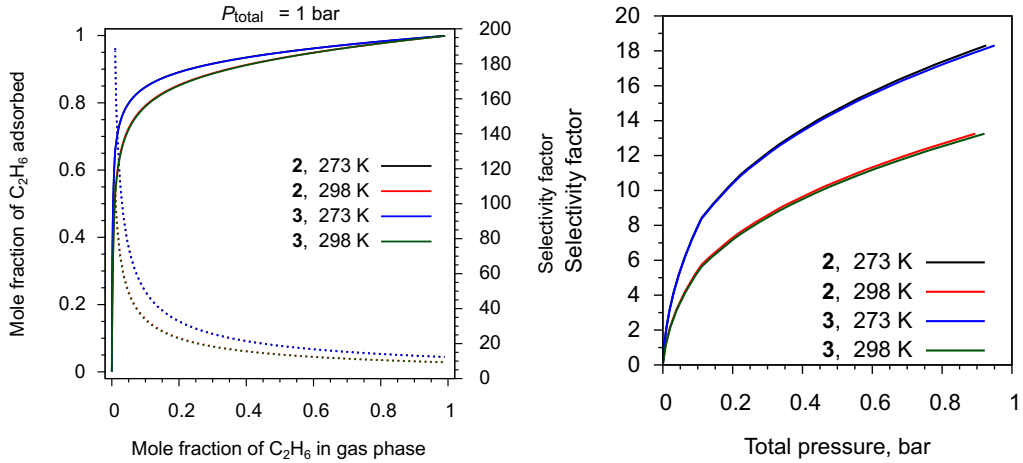

Figure S17. For binary C_2H_6/CH_4 mixture: left, prediction of adsorption equilibrium by IAST (solid lines) and dependence of selectivity factors on gas phase composition (dashed lines) at total pressure 1 bar for **2** and **3**; right, graphs of adsorption selectivity dependence on the total pressure of gases mixture for **2** and **3**.

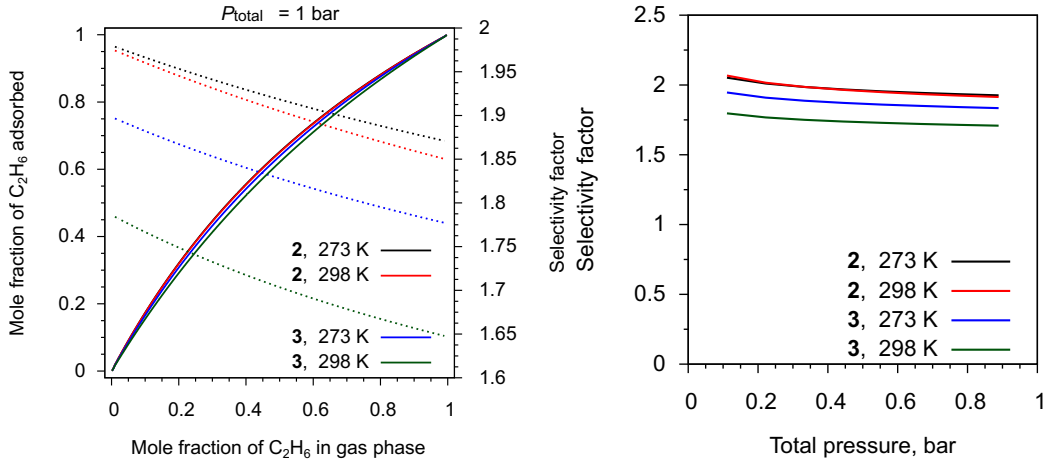

Figure S18. For binary C_2H_6/C_2H_4 mixture: left, prediction of adsorption equilibrium by IAST (solid lines) and dependence of selectivity factors on gas phase composition (dashed lines) at total pressure 1 bar for **2** and **3**; right, graphs of adsorption selectivity dependence on the total pressure of gases mixture for **2** and **3**.

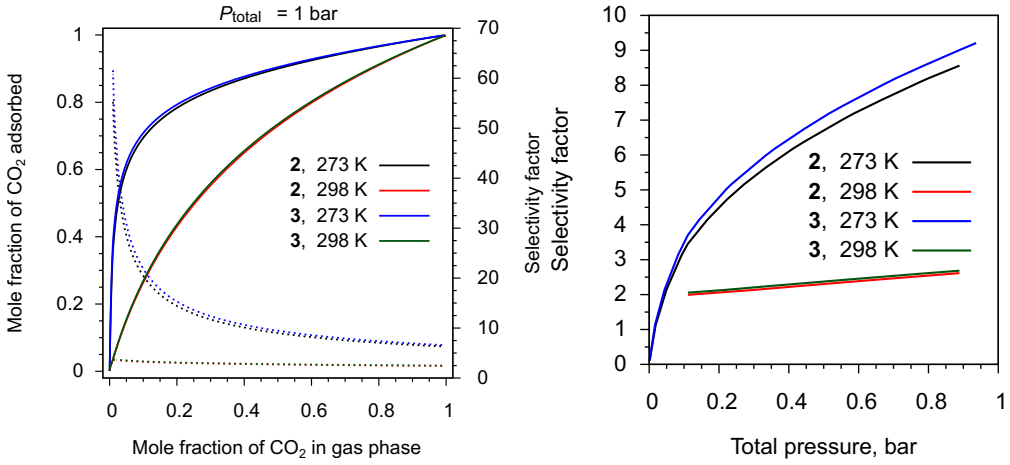

Figure S19. For binary CO_2/CH_4 mixture: left, prediction of adsorption equilibrium by IAST (solid lines) and dependence of selectivity factors on gas phase composition (dashed lines) at total pressure 1 bar for **2** and **3**; right, graphs of adsorption selectivity dependence on the total pressure of gases mixture for **2** and **3**.

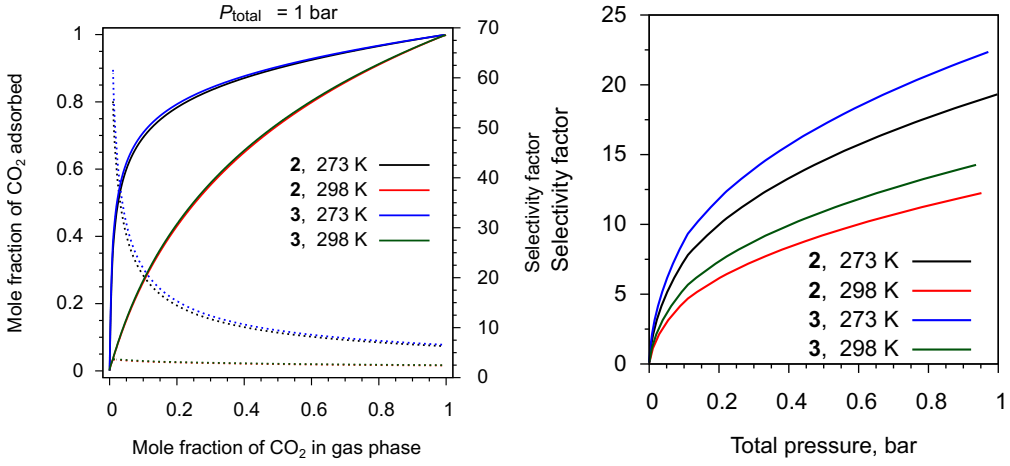

Figure S20. For binary CO_2/N_2 mixture: left, prediction of adsorption equilibrium by IAST (solid lines) and dependence of selectivity factors on gas phase composition (dashed lines) at total pressure 1 bar for **2** and **3**; right, graphs of adsorption selectivity dependence on the total pressure of gases mixture for **2** and **3**.

Table S9. For **2** and **3**, at T=273 and 298K, comparison of C_2H_6 adsorption capacity and IAST selectivity towards C_2H_6/CH_4 binary mixture on some known porous coordination cages or metal-organic frameworks.

Material	*T*, K	C_2H_2 uptake, mmol/g	C_2H_2/CH_4 IAST selectivity	Ref.
2	273	1.73	18.7	**This work**
	298	1.38	13.8	
3	273	1.77	18.5	
	298	1.37	13.6	
$Ni(tmbdc)(dabco)_{0.5}$	298	5.81	29	Ref 11
Cu-MOF	298	3.22	9.3	Ref 12
MFM-202a	293	4.21	10	Ref 13
UTSA-35a		2.43	15	Ref 14
FIR-7a-ht	298	4.06	14.6	Ref 15
JLU-Liu45	298	3.78	20.1	Ref 16
Zr-SDBA	298	2.08	15.0	Ref 17
UPC-33	273	1.56	6.64	Ref 18
FJI-H21	298	3.45	17.1	Ref 19
UPC-100-In	298	5.32	17.9	Ref 20
LIFM-26	273	4.6	11.0	Ref 21

11 Y. Wu, Z. Liu, J. Peng, X. Wang, X. Zhou, Z. Li Enhancing Selective Adsorption in a Robust Pillared-Layer Metal–Organic Framework via Channel Methylation for the Recovery of C2–C3 from Natural Gas *ACS Appl. Mater. Interfaces*, **2020**, *12*, 51499-51505.

12 S-M. Wang, Q-Y. Yang A copper-based metal-organic framework for upgrading natural gas through the recovery of C_2H_6 and C_3H_8 doi 10.1016/j.gce.2022.04.006 *in the press.*

13 S. Gao, C. G. Morris, Z. Lu, Y. Yan, H. G. W. Godfrey, C. Murray, C. C. Tang, K. M. Thoma, S. Yang, M. Schröder Selective Hysteretic Sorption of Light Hydrocarbons in a Flexible Metal–Organic Framework Material *Chem. Mater*. **2016**, *28*, 2331-2340.

14 Y. He, Z. Zhang, S. Xiang, F. R. Fronczek, R. Krishna, B. Chen A robust doubly interpenetrated metal–organic framework constructed from a novel aromatic tricarboxylate for highly selective separation of small hydrocarbons *Chem. Commun*., **2012**, 48, 6493-6495.

15 Y-P. He, Y-X. Tan, J. Zhang Tuning a layer to a pillared-layer metal–organic framework for adsorption and separation of light hydrocarbons *Chem. Commun.*, **2013**, *49*, 11323-11325.

16 X. Sun, X. Li, S. Yao, R. Krishna, J. Gu, G. Lia, Y. Liu A multifunctional double walled zirconium metal–organic framework: high performance for CO_2 adsorption and separation and detecting explosives in the aqueous phase *J. Mater. Chem. A*, **2020**, *8*, 17106-17112.

17 J. Gu, X. Sun, L. Kan, J. Qiao, G. Li, Y. Liu Structural Regulation and Light Hydrocarbon Adsorption/Separation of Three Zirconium–Organic Frameworks Based on Different V-Shaped Ligands *ACS Appl. Mater. Interfaces* **2021**, *13*, 41680-41687.

18 W. Fan, Y. Wang, Q. Zhang, A. Kirchon, Z. Xiao, L. Zhang, F. Dai, R. Wang, D. Sun An Amino-Functionalized Metal-Organic Framework, Based on a Rare $Ba_{12}(COO)_{18}(NO_3)_2$ Cluster, for Efficient C3/C2/C1 Separation and Preferential Catalytic Performance *Chem. Eur. J.*, **2018**, 24, 2137-2143.

19 P. Huang, C. Chen, M. Wu, F. Jiang, M. Hong An indium–organic framework for the efficient storage of light hydrocarbons and selective removal of organic dyes *Dalton Trans.*, *2019*, *48*, 5527-5533.

20 W. Fan, X. Wang, B. Xu, Y. Wang, D. Liu, M. Zhang, Y. Shang, F. Dai, L. Zhang, D. Sun Amino-functionalized MOFs with high physicochemical stability for efficient gas storage/separation, dye adsorption and catalytic performance *J. Mater. Chem. A*, **2018**, *6*, 24486-24495.

21 C-X. Chen, S-P. Zheng, Z-W. Wei, C-C. Cao, H-P. Wang, D. Wang, J-J. Jiang, D. Fenske, C-Y. Su A Robust Metal–Organic Framework Combining Open Metal Sites and Polar Groups for Methane Purification and CO2/Fluorocarbon Capture *Chem. Eur. J.*, **2017**, 23, 4060-4064.

Table S10. Comparison of C_2H_2 adsorption capacity and IAST selectivity towards C_2H_2/CH_4 binary mixture on some known porous coordination cages, porous organic cages (POC) and metal-organic frameworks

Material	***T*, K**	**C_2H_2 uptake, mmol/g**	**C_2H_2/CH_4 IAST selectivity**	**Ref.**
2	273	2.25	18.3	**This work**
	298	1.61	11.9	
3	273	2.37	19.5	
	298	1.67	12.8	
TTD-based POC[a]	273	1.61	26.2	Ref 22
ZJU-199	290	5.71	27.3	Ref 23
ZJNU-111	298	5.51	18.8	Ref 24
ZJNU-112	298	2.86	14.1	Ref 24
ZJNU-114	298	5.91	21.9	Ref 24
UMCM-150	298	5.49	19.5	Ref 24
HOF-5a	296	4.55	13.6	Ref 24
Zr-SDBA	298	4.52	230.5	Ref 17

[a] TTD = 3,3′′,5,5′′-tetraformyl-4,4′′-[1,1′:4′,1′′-terphenyl]diol

22 W. Yang, N. Sun, X. Wang, B. Yu, H. Wang Racemic Porous Organic Cage Crystal with Selective Gas Adsorption Behaviors *Z. Anorg. Allg. Chem.* **2022**, *648*, e202100357.

23 L. Zhang, C. Zou, M. Zhao, K. Jiang, R. Lin, Y. He‖, C-D. Wu, Y. Cui, B. Chen, G. Qian Doubly Interpenetrated Metal–Organic Framework for Highly Selective C_2H_2/CH_4 and C_2H_2/CO_2 Separation at Room Temperature *Cryst.Growth Des*. **2016**, *16*, 7194-7197.

24 H. Wang, B. Li, H. Wu, T-L. Hu, Z. Yao, W. Zhou, S. Xiang, B. Chen A Flexible Microporous Hydrogen-Bonded Organic Framework for Gas Sorption and Separation *J. Am. Chem. Soc*. **2015**, *137*, 9963-9970.